

# Characterization of nanoscale features in tapered fractal and photonic crystal fibers

C. M. Rollinson,<sup>1</sup> S. T. Huntington,<sup>1</sup> B. C. Gibson,<sup>1,\*</sup> S. Rubanov,<sup>2</sup> and J. Canning<sup>3</sup>

<sup>1</sup>*School of Physics, The University of Melbourne, Parkville, Victoria, 3010, Australia*

<sup>2</sup>*Bio21 Institute, The University of Melbourne, Parkville, Victoria, 3010, Australia*

<sup>3</sup>*Interdisciplinary Photonics Laboratories, School of Chemistry, The University of Sydney, 206 National Innovation Centre, Eveleigh, New South Wales, 1430, Australia*

\*[b.gibson@unimelb.edu.au](mailto:b.gibson@unimelb.edu.au)

**Abstract:** The internal structure of nanostructured air-silica fiber probes have been characterized using a combined focused ion beam and scanning electron microscopy technique. The collapse rate of the air-holes is shown to differ substantially between a regular photonic crystal fiber (PCF) and the quasi-periodic Fractal fiber. The integrity of the Fractal fiber structure is maintained down to an outer diameter as small as 120 nm, whereas the air-holes of the regular PCF begin to collapse when the outer diameter is approximately 820 nm. The observed smallest hole diameter of 10 nm is suggested to be due to physical limits imposed by the molecular structure of silica. These results confirm structural inferences made in previous publications.

©2011 Optical Society of America

**OCIS codes:** (060.2280) Fiber design and fabrication; (060.4005) Microstructured fibers; (060.5295) Photonic crystal fibers; (180.4243) Near-field microscopy; (180.5810) Scanning microscopy; (060.2350) Fiber optics imaging; (050.1220) Apertures; (050.1940) Diffraction.

---

## References and links

1. L. M. Tong, R. R. Gattass, J. B. Ashcom, S. He, J. Lou, M. Shen, I. Maxwell, and E. Mazur, "Subwavelength-diameter silica wires for low-loss optical wave guiding," *Nature* **426**(6968), 816–819 (2003).
2. P. Russell, "Photonic crystal fibers," *Science* **299**(5605), 358–362 (2003).
3. T. M. Monro, D. J. Richardson, N. G. R. Broderick, and P. J. Bennett, "Holey optical fibers: an efficient modal model," *J. Lightwave Technol.* **17**(6), 1093–1102 (1999).
4. J. K. Ranka, R. S. Windeler, and A. J. Stentz, "Visible continuum generation in air-silica microstructure optical fibers with anomalous dispersion at 800 nm," *Opt. Lett.* **25**(1), 25–27 (2000).
5. B. C. Gibson, S. T. Huntington, S. Rubanov, P. Olivero, K. Digweed-Lyytikäinen, J. Canning, and J. D. Love, "Exposure and characterization of nano-structured hole arrays in tapered photonic crystal fibers using a combined FIB/SEM technique," *Opt. Express* **13**(22), 9023–9028 (2005), <http://www.opticsinfobase.org/oe/abstract.cfm?URI=oe-13-22-9023>.
6. T. A. Birks, J. C. Knight, and P. S. Russell, "Endlessly single-mode photonic crystal fiber," *Opt. Lett.* **22**(13), 961–963 (1997).
7. J. K. Chandalia, B. J. Eggleton, R. S. Windeler, S. G. Kosinski, X. Liu, and C. Xu, "Adiabatic coupling in tapered air-silica microstructured optical fiber," *IEEE Photon. Technol. Lett.* **13**(1), 52–54 (2001).
8. S. T. Huntington, J. Katsifolis, B. C. Gibson, J. Canning, K. Lyytikäinen, J. Zagari, L. W. Cahill, and J. D. Love, "Retaining and characterising nano-structure within tapered air-silica structured optical fibers," *Opt. Express* **11**(2), 98–104 (2003), <http://www.opticsinfobase.org/oe/abstract.cfm?URI=oe-11-2-98>.
9. E. C. Mägi, P. Steinvurzel, and B. J. Eggleton, "Tapered photonic crystal fibers," *Opt. Express* **12**(5), 776–784 (2004), <http://www.opticsinfobase.org/oe/abstract.cfm?URI=oe-12-5-776>.
10. Y. Youk, D. Y. Kim, and K. W. Park, "Guiding properties of a tapered photonic crystal fiber compared with those of a tapered single-mode fiber," *Fiber Int. Opt.* **23**(6), 439–446 (2004).
11. Y. K. Lizé, E. C. Mägi, V. G. Ta'eed, J. A. Bolger, P. Steinvurzel, and B. J. Eggleton, "Microstructured optical fiber photonic wires with subwavelength core diameter," *Opt. Express* **12**(14), 3209–3217 (2004), <http://www.opticsinfobase.org/oe/abstract.cfm?URI=oe-12-14-3209>.
12. H. C. Nguyen, B. T. Kuhlmeier, E. C. Magi, M. J. Steel, P. Domachuk, C. L. Smith, and B. J. Eggleton, "Tapered photonic crystal fibers: properties, characterisation and applications," *Appl. Phys. B* **81**(2-3), 377–387 (2005).
13. C. Kerbage, and B. J. Eggleton, "Tunable microfluidic optical fiber gratings," *Appl. Phys. Lett.* **82**(9), 1338–1340 (2003).
14. S. G. Leon-Saval, T. A. Birks, W. J. Wadsworth, P. St. J. Russell, and M. W. Mason, "Supercontinuum generation in submicron fibre waveguides," *Opt. Express* **12**(13), 2864–2869 (2004), <http://www.opticsinfobase.org/oe/abstract.cfm?URI=oe-12-13-2864>.

15. B. H. Lee, J. B. Eom, J. Kim, D. S. Moon, U.-C. Paek, and G.-H. Yang, "Photonic crystal fiber coupler," *Opt. Lett.* **27**(10), 812–814 (2002).
16. T. A. Birks, G. Kakarantzas, P. S. J. Russell, and D. F. Murphy, "Photonic crystal fiber devices," *Proc. SPIE - Int. Soc. Opt. Eng.* **4943**, 142–151 (2003).
17. C. Martelli, and J. Canning, "Fresnel Fibers for Sensing," in *Optical Fiber Sensors*, (Cancun, Mexico 2006) OSA Technical Digest (CD) (Optical Society of America), 2006; post-deadline paper ThF5.
18. G. S. Wiederhecker, C. M. B. Cordeiro, F. Couny, F. Benabid, S. A. Maier, J. C. Knight, C. H. B. Cruz, and H. L. Fragnito, "Field enhancement within an optical fibre with a subwavelength air core," *Nat. Photonics* **1**(2), 115–118 (2007).
19. J. Kim, and K.-B. Song, "Recent progress of nano-technology with NSOM," *Micron* **38**(4), 409–426 (2007).
20. S. T. Huntington, B. C. Gibson, J. Canning, K. Digweed-Lyytikäinen, J. D. Love, and V. Steblina, "A fractal-based fibre for ultra-high throughput optical probes," *Opt. Express* **15**(5), 2468–2475 (2007), <http://www.opticsinfobase.org/oe/abstract.cfm?URI=oe-15-5-2468>.
21. C. M. Rollinson, S. M. Orbons, S. T. Huntington, B. C. Gibson, J. Canning, J. D. Love, A. Roberts, and D. N. Jamieson, "Metal-free scanning optical microscopy with a fractal fiber probe," *Opt. Express* **17**(3), 1772–1780 (2009), <http://www.opticsexpress.org/abstract.cfm?URI=oe-17-3-1772>.
22. C. Martelli, J. Canning, B. C. Gibson, and S. T. Huntington, "Bend loss in structured optical fibres," *Opt. Express* **15**(26), 17639–17644 (2007), <http://www.opticsinfobase.org/oe/abstract.cfm?URI=oe-15-26-17639>.
23. W. J. Wadsworth, A. Witkowska, S. G. Leon-Saval, and T. A. Birks, "Hole inflation and tapering of stock photonic crystal fibres," *Opt. Express* **13**(17), 6541–6549 (2005), <http://www.opticsinfobase.org/oe/abstract.cfm?URI=oe-13-17-6541>.
24. G. A. Valaskovic, M. Holton, and G. H. Morrison, "Parameter control, characterization, and optimization in the fabrication of optical fiber near-field probes," *Appl. Opt.* **34**(7), 1215–1228 (1995).
25. A. C. Wright, "Defect-free vitreous networks: The idealised structure of SiO<sub>2</sub> and related glasses," in *Defects in SiO<sub>2</sub> and Related Dielectrics: Science and Technology*, G. Pacchioni, L. Skuja, and D. L. Griscom, eds. (Kluwer Academic Publishers, Dordrecht, the Netherlands, 2000).

## 1. Introduction

The development of truly nanostructured fibers, tapers and optical wires holds exciting potential in many applications with increasing demand for the miniaturization of glass-based photonic components. Silica nanowires, with diameters as small as 50 nm, have been demonstrated for low loss optical waveguiding [1]. Photonic crystal fibers (PCFs) [2] are also known as holey fibers [3] or microstructured fibers [4] and more generally structured fibers since the features can be nano [5]. PCFs are typically manufactured using a technique of stacking silica capillary tubes of equal size in a hexagonal lattice pattern [6]. Such fibers are usually characterized by a regular, periodic array of microscopic air-holes in the cladding region which exist along their entire fiber length. The tapering of structured fibers has attracted much interest [7–12], with many applications including microfluidics [13], enhancement of non-linear properties [14], couplers [15] and low-loss transition to conventional optical fibers [16]. The possibility that the evanescent optical field itself can be tailored on such dimensions also exists – the accumulation of the evanescent field, for example, can exceed the surrounding optical field when the hole is sufficiently small despite the low index of silica [17,18]. This potentially promises a new class of nanophotonics devices exploiting such high resolution optical localisation. In this paper, we explore the production of nanostructured holes down to 10nm or less. We compare to types of optical structured fibres to see how they impact the evolution of the hole and the degree of control possible by varying the starting geometry. One is a conventional periodic structured fibre with an array of channels whilst the other is a so-called fractal fibre where the triangular lattice self-images to decreasing size towards the centre of the fibre.

Recently, we investigated the fractal fibre as a potential scanning near-field optical microscopy (SNOM) probe [19]. Unlike a typical PCF, the holes in a Fractal fibre are neither in a periodic array nor radially aligned. The cross-sectional area of the holes in a Fractal fibre increase in size with distance from the centre of the fibre and each consecutive ring of holes is rotated by  $\pi/n$ , where  $n$  is the number of holes in each ring. As a result of its unique design, the Fractal fibre has been shown to exhibit superior optical throughput and high numerical aperture (NA) compared to a regular PCF and a standard step-index fiber SNOM probes [20]. A metal-free Fractal fiber probe has also demonstrated an enhanced capacity for collection mode imaging of a metallic nanostructure in comparison to uncoated and metal-coated standard step-index fiber probes [21]. The unique quasi-periodic structure of the Fractal fiber

has also been shown to lead to almost zero bend loss across a wide wavelength range [22]. For SNOM probes which are manufactured from structured optical fibre such as the Fractal fibre, retaining the internal nanostructure along the tapered probe becomes critical for the optimal confinement of light to or from the tip. Enhanced optical confinement within the fibre leads to minimal interaction with the surrounding metal-coating, which is typically used, and reduces attenuation. The ability to examine, monitor and confirm the internal structure of tapered structured SNOM probes will provide further insight into the optical confinement properties of the probe. What stood out in this work was the ability to retain open channels in a controlled way down to small sizes, entering the nano domain  $<100\text{nm}$ . A number of techniques have been proposed for characterizing the structure of the cleaved end-face of air-silica fiber tapers, including optical microscopy [7] and scanning electron microscopy (SEM) [9,12]. Atomic force microscopy (AFM) has been used to characterize an adiabatically tapered air-silica fiber with an outer diameter (OD) of  $15\ \mu\text{m}$  [8] and detected air-holes with approximate diameters of  $400\ \text{nm}$ . These holes were approximately 10% smaller than expected, providing evidence of hole collapse due to surface tensions within the holes [23]. Air-silica tapers with ODs as small as  $1.6\ \mu\text{m}$  have been characterized using a combined focused ion beam (FIB)/SEM technique [5] to reveal air-holes as small as  $60\ \text{nm}$  in diameter. In this paper, in order to explore just how small we can go with the holes in the two types of fibre, a combined FIB/SEM technique is used to characterize the degree to which the internal structures of the regular PCF and the fractal fiber are maintained along a tapered probe. The results presented quantify the minimum hole sizes in both of the tapered fibre types and provide further insight into the possible limits enhanced optical confinement and collection properties these fibres.

## 2. Tapered probe fabrication and characterization

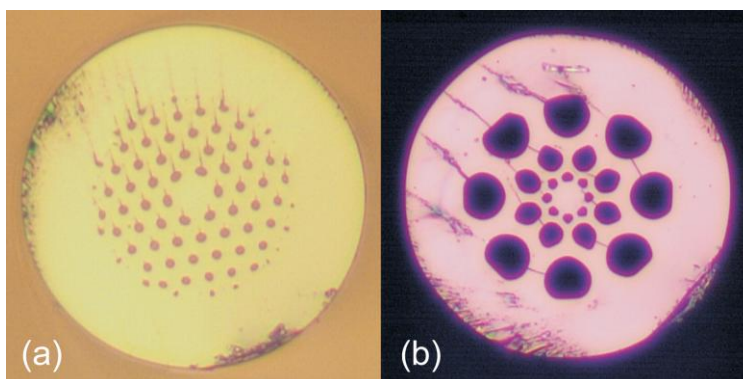


Fig. 1. Optical micrographs of the cleaved end-face of the untapered (a) regular PCF with an OD of  $100\ \mu\text{m}$  and (b) Fractal fiber with an OD of  $125\ \mu\text{m}$  [18].

Microscope images of the two structured fibers considered are shown in Fig. 1: (a) a regular PCF with an OD,  $\Lambda = 100\ \mu\text{m}$  and (b) the Fractal fiber with  $\Lambda = 125\ \mu\text{m}$ . The regular PCF consists of a 4-layer hexagonal lattice of 60 holes with approximate initial diameters and pitch,  $\Lambda = 2.5\ \mu\text{m}$  and  $6.75\ \mu\text{m}$ , respectively. The initial air-hole diameters in rings 3, 2 and 1 of the Fractal fibre are approximately  $\Lambda = 16\ \mu\text{m}$ ,  $8\ \mu\text{m}$  and  $4\ \mu\text{m}$ , respectively, where ring 3 is the outermost ring. The Fractal fiber has been designed specifically for tapering such that as the diameter is reduced along a taper, the modal field remains confined within the structured region by a successive ring of holes as the inner ring becomes optically insignificant. The larger holes of the Fractal fiber increase the air fraction substantially which also acts to enhance confinement and reduce optical loss in tapered probes. Whether this translates to eventually producing smaller holes with greater finesse is unclear.

The regular PCF and Fractal fiber probes were fabricated at room temperature using a  $\text{CO}_2$ -laser-based pulling method [24] during which no additional gas was used to pressurize

the air-holes; a method that can be used to prevent hole collapse [23]. The probes were then coated with approximately 30 nm of gold to prevent charging during SEM imaging. The probes were milled using a FEI Nova Dualbeam FIB and SEM system which provided a 30 kV Ga<sup>+</sup> ion beam with a current of approximately 30 pA and a spot size of around  $\omega = 20$  nm. A number of FIB 'slices' (or cleaves) were made across the probes, i.e. perpendicular to the longitudinal direction of the taper. FIB slices were made as close as possible to the probe tips and SEM imaging was performed immediately after cleaving to reveal the cross-sections of the structured fiber probes. Various slices, corresponding to increments of approximately  $\Delta z = 100$  nm in the OD of the taper, were performed on the probes and the SEM images are shown in Figs. 2 and 3 for the PCF and Fractal fibre, respectively.

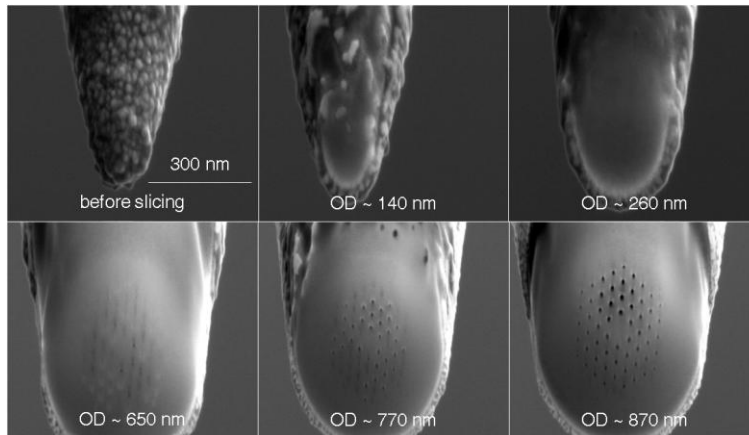


Fig. 2. SEM images recorded before and after FIB slices were made on a single regular PCF tapered probe. The entire structure of air-holes is visible at  $\Delta z = 870$  nm. All OD values are estimated to be accurate to within  $\pm 10$  nm. All images were recorded at different magnifications.

Repeated FIB slices performed on the regular PCF probe did not begin to reveal any air-holes until the OD reached approximately  $\Delta z = 360$  nm. However, even at  $\Delta z = 650$  nm, the majority of the air-holes had collapsed as shown in Fig. 2. The entire structure of air-holes was not revealed until  $\Delta z \sim 870$  nm. The images in Fig. 2 indicate that air-hole collapse began to occur at an OD between 770 nm and 870 nm, or at approximately  $\Delta z = (820 \pm 50)$  nm. The smallest air-hole diameter measured in the images was approximately  $\Delta z = 10$  nm and the evolution of the average air-hole diameters over the entire array of 60 holes in the regular PCF probe is shown in Fig. 4. In the absence of external influences, air-hole diameters are expected to approach zero with the taper OD. The plot in Fig. 4 clearly demonstrates premature collapse of the PCF air-holes since the average diameters move toward zero well before expected. This apparent air-hole collapse is possibly due to surface tension within the holes. Furthermore, as the holes were so small, it is also possible that the energy of the beam caused apparent collapse during FIB slicing. However, based on the geometry of the taper profiles, shown in [5,18,19], an OD of 820 nm is estimated to correspond to a distance of approximately 6  $\mu\text{m}$  from the probe tip. This result is consistent with previous work that demonstrated significant optical leakage at a similar distance from the tip of a similar PCF probe [18]. Therefore surface tension within the holes is likely to be a major cause of the observed premature air-hole collapse. Consequently, a tapered larger air-fraction regular PCF is expected to collapse at a rate proportional to the OD since larger air-holes will provide greater resistance to surface tension within the holes.

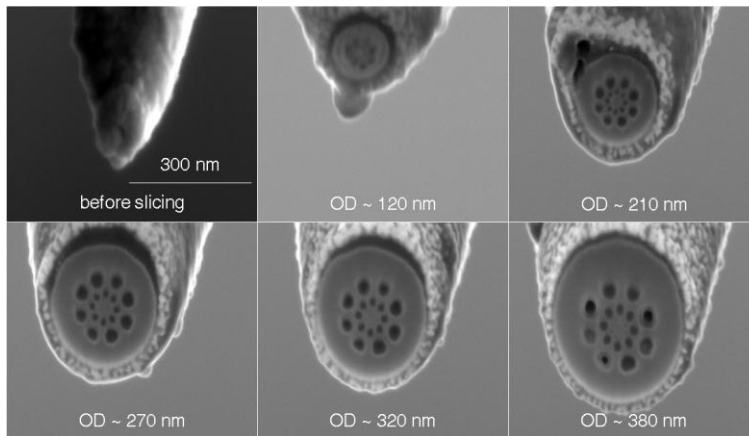


Fig. 3. SEM images recorded before and after FIB slices were made on a single Fractal fiber tapered probe. The entire structure of air-holes is clearly visible at an OD of approximately 425 nm. It should be noted that the entire structure of air-holes for the regular PCF is not visible until the OD is  $\sim 870$  nm. All OD values are estimated to be accurate to within  $\pm 10$  nm. All images were recorded at different magnifications.

Various FIB slices performed on the Fractal fiber tapered probe indicate that the outer ring of air-holes remains open along the taper at least to an OD of 120 nm, as shown in Fig. 3. The next SEM image taken after FIB slicing the same Fractal probe shows the outer two rings of air-holes open at an OD of 210 nm. From previously reported work [18], a taper OD of 210 nm is estimated to correspond to a distance of approximately  $1 \mu\text{m}$  from the tip. The ability to monitor and confirm that nanoscale structures exist within the Fractal probe with ODs less than  $\lambda = 200$  nm supports reported enhanced optical throughput and collection results [18,19]. Subsequent FIB slices made to the Fractal probe confirmed that the internal structure of the fiber was maintained along the taper. The entire Fractal fiber structure is clearly visible when the taper OD is approximately  $\lambda = 425$  nm. Figure 4 shows the evolution of the average air-hole diameters in the Fractal fiber probe as a function of OD. The smallest air-hole diameter measured in the images of the Fractal fiber probe was approximately  $\lambda = 10$  nm. The progressions of the air-hole diameters in all three rings show linear trends and least squares fits to the data show near-zero intercepts, indicating minimal signs of premature hole collapse. The images recorded after FIB slicing were performed on both the regular PCF and Fractal fiber probes revealed minimum air-hole diameters of approximately  $\lambda = 10$  nm, despite the vastly different rates of collapse shown in Fig. 4 for all hole sizes. This indicates that there is a physical limit after which imminent collapse begins to occur when the hole diameter reaches this size, shown as a dashed line in Fig. 4. We postulate that this may be due to the material regime where long range disorder no longer dominates – rather, short range and intermediate range order changes the response of the macroscopic homogenous glass system. At these dimensions, local nanocavities are also present. From observed correlation patterns for x-ray and neutron diffraction scattering studies of vitreous silica, short range order (determined by the tetrahedral silica structure) is readily observed to 1-2 nm [25], depending on the glass preparation and the resultant ring sizes within the network. Since correlation implies local strains determined by local geometry, structures that start to approach this range are subject to forces which are negligible on a macroscale. These results provide evidence for a new boundary reached by decreasing nanostructures within amorphous materials such as silica. Below this boundary could be considered an “intermolecular collapse zone (ICZ)” for features in silica which marks the onset of intermolecular stereo strains that can no longer be ignored.

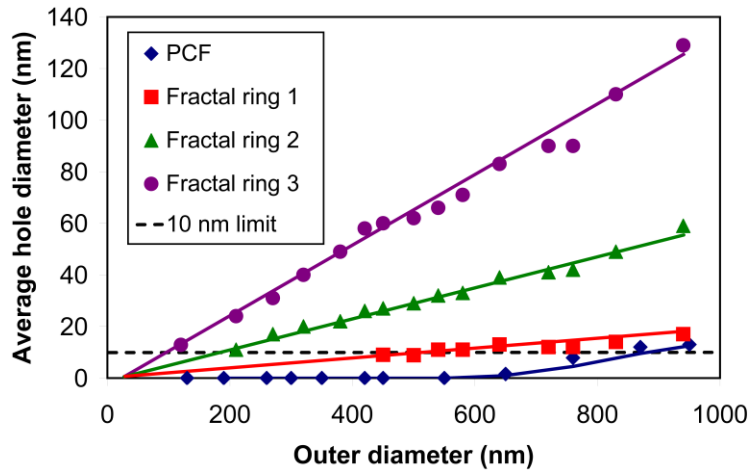


Fig. 4. The evolution of average air-hole diameters versus the outer diameter of the regular PCF and the Fractal fiber probes. Error bars are not shown as they are smaller than the data points.

### 3. Conclusions

The evolution of nanostructured holes within the tips of tapered regular PCF and Fractal fiber probes have been monitored and compared using a combined FIB/SEM technique. The SEM images clearly show a demonstrated ability to fabricate and control nanostructured materials in air-silica fibers. The air-holes in a regular PCF tapered probe were shown to be maintained to an OD of  $\bar{A} = (870 \pm 10)$  nm. Further characterization of regular PCF tapers for smaller ODs, closer to the tip, depicted hole collapse which can be attributed to surface tension within the holes. The entire structure of the Fractal fiber was shown to be maintained down to an OD of  $\bar{A} = (425 \pm 10)$  nm. The outer ring of air-holes in the Fractal fiber structure is maintained to an OD of  $(120 \pm 10)$  nm. In contrast to the regular array PCF, within the fractal fibre, regardless of the initial hole size, the rate of collapse scales with the outer diameter, indicating the use of larger outer diameters can permit greater degree of control. The capability to monitor and confirm that nanoscale structures exist within the Fractal probe with ODs less than 200 nm corroborates reported enhanced optical throughput and collection results [18,19]. Using a larger air-fraction regular PCF is likely to keep the air-holes open longer along a tapered probe but such fibers are not expected to provide the superior confinement properties or versatility of the scale invariant Fractal fiber structure – therefore, the choice of fibre design is ultimately influenced by the intended application. The observation of a small hole size limit of  $\sim 10$  nm in both tapered structured fibers may represent the onset of strain imposed by local order and local ring distributions within the glass. Further work is currently being undertaken to explore the hole size dependency on the preparation of glass materials. Such a limit suggests a regime well into the nano-domain that may present new barriers and challenges for genuine design engineering to molecular dimensions via a top down approach. At the same time, a new platform for testing theories on the glassy state particularly where the boundaries are defined, as well as providing new insights, is available.

### Acknowledgements

The support of the Australian Research Council, through its Discovery and Centres of Excellence programs (DP0877871), is gratefully acknowledged. The authors would also like to acknowledge M. Stevenson, K. Digweed-Lyytikainen, V. Steblina, J. Digweed, J. Zagari and B. Ashton for their assistance with fiber preparation and useful discussions.